

Stability of constrained cylindrical interfaces and the torus lift of Plateau–Rayleigh

J. B. BOSTWICK¹ AND P. H. STEEN^{2†}

¹Department of Theoretical and Applied Mechanics, Cornell University, Ithaca, NY 14853, USA

²School of Chemical and Biomolecular Engineering and Center for Applied Mathematics, Cornell University, Ithaca, NY 14853, USA

(Received 16 September 2009; revised 2 December 2009; accepted 3 December 2009)

Surface tension acting at a cylindrical interface holds an underlying liquid in motionless equilibrium. This static base state is subject to dynamic capillary instability, including Plateau–Rayleigh breakup. If the interface is partially supported by a cylindrical cup-like solid, the extent of the wetting contact can significantly influence the dynamics and the stability of the configuration. The equation for the motion of small disturbances is formulated as an eigenvalue equation on linear operators. A solution is constructed on a constrained function space using a Rayleigh–Ritz procedure. The influence of the extent-of-constraint on the dispersion relation and on modal structures is reported. In the extreme, the support reduces to a wire, aligned axially, and just touching the interface. From prior work, this constraint is known to stabilize the Plateau–Rayleigh limit by some 13%. We report the wavenumber of maximum growth and estimate the time to breakup. The constraint is then bent in-plane to add a weak secondary curvature to the now nearly cylindrical base state. This is referred to as the torus lift of the cylinder. The static stability of these toroidal equilibria, calculated using a perturbation approach, shows that the position of constraint is crucial – constraint can stabilize (outside) or destabilize (inside). The combined influence of secondary curvature and wire constraint on the Plateau–Rayleigh limit is tracked. Finally, attention is restricted to constraints that yield a lens-like cylindrical meniscus. For these lenses, the torus lift is used as apparatus along with a symmetrization procedure to prove a large-amplitude static stability result. Our study is conveniently framed by a classic paper on rivulets by Davis (*J. Fluid Mech.*, vol. 98, 1980, p. 225).

1. Introduction and background

A liquid cylinder can break up due to the force of surface tension. By comparing surface areas of the disturbed and the undisturbed base-state shape, a thermodynamic approach, Plateau (1863) found instability of the cylinder for lengths longer than the base-state circumference, the well-known Plateau limit. Plateau went on to *incorrectly* interpret this limit as predicting the size of drop resulting from the instability. By solving the dynamical governing equations, the hydrodynamic approach, Rayleigh (1879) calculated the growth rate as it depends on disturbance wavenumber and *correctly* interpreted the wavenumber of maximum growth rate from this dispersion relation as giving a good approximation to the final drop size. The Plateau limit

† Email address for correspondence: phs7@cornell.edu

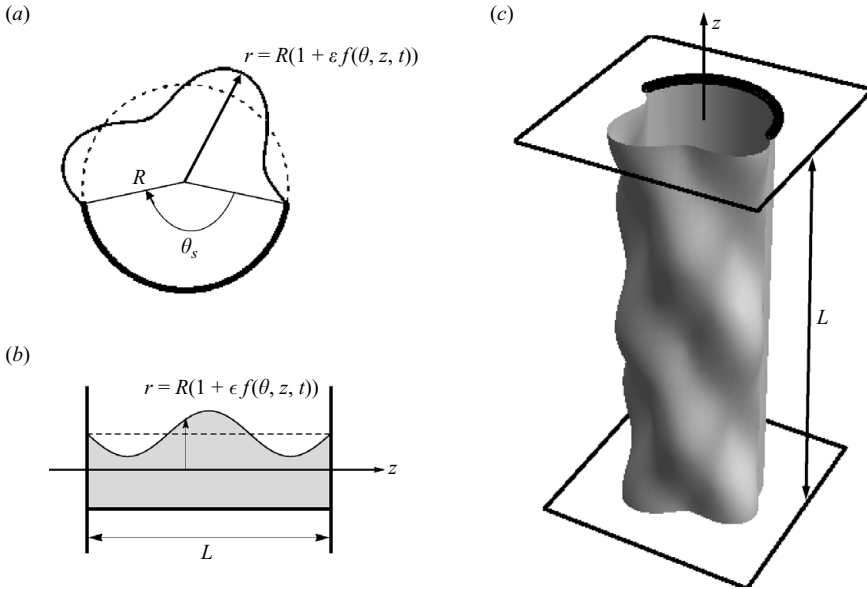


FIGURE 1. Definition sketch (a) cross-section with solid support (thick), (b) axial section with interface pinned at endpoints and (c) three-dimensional view, with sample disturbed interface.

is recovered from the Rayleigh result by putting growth rate to zero. Probably for this reason, the Plateau limit is sometimes referred to as the Plateau–Rayleigh limit. Henceforth in this paper, ‘thermostatic’ and ‘hydrodynamic’, terminology used by Davis (1980) to distinguish the different approaches, will be shortened to ‘static’ and ‘dynamic’.

Constrained capillary interfaces are important in a number of applications including coating and casting processes, low-gravity liquid containment and two-phase heat transfer. In planar-flow spin-casting, for example, molten metal is held by surface tension between a stationary nozzle and a moving substrate (Steen & Karcher 1997). The upstream meniscus is nearly cylindrical and is part of a full meniscus which takes the shape of a distorted torus. Both meniscus interfaces are constrained by contact with the nozzle surface above and substrate below. Inviscid capillary oscillations can get frozen into the ribbon product as defects. Indeed, stable Rayleigh vibrations of a sphere held by surface tension capture the wavelength of the defect (Byrne *et al.* 2006). The constrained toroidal geometry used here is potentially relevant to the drop impact problem of Renardy *et al.* (2003), where a toroidal rim, attached to a thin liquid sheet is formed after impact. Similarly, the formation of Edgerton crowns, or the ‘crown-splash problem’, result from instability of toroidal rims (see Deegan, Brunet & Eggers 2008). In low-gravity environments, it is the weight penalty associated with the solid container that has led to consideration of wire-frame forms for liquid containment (Lowry & Thiessen 2007). Mass transfer advantages may also accrue (Thiessen, Bernate & Marston 2005). Finally, rivulets of liquids on solid surfaces, whose stability is important to heat transfer applications, can be viewed as constrained cylinder-like interfaces (Davis 1980; Weiland & Davis 1981).

We study the stability of cylindrical interfaces constrained by wetting contact with a cylindrical cup of circular cross-section (figure 1). The interface is pinned at contact

lines along the edges of the solid support. The polar angle of contact θ_s defines the extent of the cylindrical-cup constraint. First, using the dynamic approach for inviscid liquids, we calculate the modes of instability and dispersion relations for $0 < \theta_s < 2\pi$, extending previous results obtained by the static approach, much as Rayleigh extended the Plateau result. Next, we bend the cylindrical interface by requiring wetting against a toroidal-cup constraint, thereby introducing a weak secondary curvature. That is, we consider toroidal interfaces near the cylindrical limit. Unlike the cylinder, the torus is not an equilibrium shape but there exists a near-torus equilibrium shape whose cross-sections are deformed circular arcs. Using a perturbation approach, we calculate the static stability of these base states, showing that the constraint can either stabilize or destabilize depending on its inside or outside position. Moreover, in the case of stabilization, we identify a base shape for which the destabilization of the secondary curvature just cancels the stabilization by the wire constraint. That is, the Plateau limit is lifted to the torus. Finally, using the static approach on the torus lift of the cylinder, we show that $\theta_s = \pi$ bounds a stability window where here stability is to *finite-amplitude* disturbances. The argument uses a symmetrization procedure that goes back to Steiner (1882).

The influence of constraints, such as wetting conditions and substrate geometry, on the Plateau–Rayleigh problem is relevant to capillary jets, liquid bridges, columns, ridges and fillet beads, among others. The literature has a long history (Lamb 1932) and has grown to be vast. We shall focus on nearly cylindrical interfaces and mention only a few of the most relevant studies. The static approach is reviewed by Michael (1981), while derivations for both the static and dynamic approach along with an assembly of problems are found in the book by Myshkis *et al.* (1987).

In a study of two-dimensional pendant drops with translational symmetry, Majumbar & Michael (1976) obtain the static stability of a cylindrical meniscus pinned along a horizontal slot, as a limiting case. Brown & Scriven (1980) consider the exactly cylindrical fillet for constant-pressure as well as constant-volume disturbances and report static stability. In a study of moving contact lines and rivulets, Davis (1980) considers the stability of a static rivulet of circular-arc cross-section on a horizontal plate. Davis obtains useful results from a dynamical formulation, without solving the eigenvalue problem, before recovering a number of static results. Langbein (1990) treats the static stability of cylindrical interfaces constrained to wet a V-groove, considering liquid in positions both inside and outside the groove. Roy & Schwartz (1999) also study liquids that partially wet cylindrical ‘containers’ of a variety of cross-sectional shapes, including planar, V-groove, circular and elliptical. Their static stability analyses of the circular-arc cross-section base-state recover results of the previous studies and also treat some new substrate geometries. May & Lowry (2008) propose helical and double-helical wire constraints (pinning locus) to support liquid columns and calculate the static stability of resulting interfaces, which may or may not be nearly cylindrical. Despite the variety of these base states, the stability of the toroidal base state has not been considered before, as far as we are aware.

As regards relevant dynamic stability studies, Myshkis *et al.* (1987) (§5.3.4) sketch one solution approach for vibrations of an ideal liquid underlying a cylindrical meniscus supported by a V-groove with convex circular bottom, all for natural boundary conditions (contact angle of $\pi/2$). No dispersion relations or eigenmodes are presented. Static results are recovered: axial disturbances are unstable at half the Plateau–Rayleigh limit and planar disturbances for base-state interfaces greater than semicircular.

The Davis (1980) study of static rivulets conveniently frames our study even though the moving contact line is not the interest of our paper. His cylindrical base state has contact lines that are plane and parallel and move (or not) under disturbance according to one of a number of alternative contact line models, including the pinned model (non-moving). Our cylindrical interface base state is identical to Davis' pinned rivulet base state. Davis uses the dynamic approach. Without solving them, Davis manipulates the linearized stability equations to obtain a balance equation for disturbance energy that takes the form of a damped linear-harmonic-oscillator equation, of the same form – remarkably – for all the contact line models he considers (adapted to our notation),

$$M\sigma^2 + \Phi\sigma + K = 0. \quad (1.1)$$

Here σ is the linear-stability-theory growth rate, $M > 0$ is the disturbance kinetic energy, $\Phi \geq 0$ is the viscous dissipation and K is the interfacial energy. For inviscid flow $\Phi = 0$, all disturbances oscillate without growth for $K > 0$ (stability) and some grow without bound for $K < 0$ (instability). Furthermore, $K = 0$ yields the stability boundary obtained by the static approach. Davis analyses the functional K as a function of scaled axial wavenumber α to find boundaries of windows of instability,

$$\alpha_c^2 = 1 - \pi^2 / (2\pi - \theta_s)^2. \quad (1.2)$$

For example, $\theta_s = 0$ corresponds to the limiting case of a cylindrical interface touching the plane along a generator line and yields an upper boundary of $\alpha_c = (3/4)^{1/2}$ (note that the Plateau limit $\alpha_c = 1$ cannot be recovered from (1.2) because of differences in the class of disturbances admitted). In contrast, $\theta_s > \pi$ is a lens-like cylindrical interface resting on a parallel plane; this case is seen to be stable to all lengths. Davis' stability limits recover the constant-volume limits of Brown & Scriven (1980) and Majumbar & Michael (1976), as expected.

We solve the disturbance equations posed by Davis in the case of an inviscid fluid to obtain explicit dispersion relations $\sigma^2(\alpha)$ as well as eigenmode structures, consistent with (1.1). An integrodifferential boundary value problem on the interface deflection is derived for both natural and pinned axial end-plane conditions. Here, the interface is defined as the union of the free-surface and cup support. A solution is constructed by reformulating the governing equation as an eigenvalue problem on linear operators, followed by a Rayleigh–Ritz procedure on a constrained function space. A similar method has been used by Bostwick & Steen (2009) for a constrained sphere. The incorporation of constraints into an appropriate function space is not new, but has been previously limited to problems with symmetry. For example, Lyubimov, Lyubimova & Shklyaev (2006) exploit the symmetry of an oscillating hemispherical drop on a plate to study contact line dynamics. For constrained problems without symmetry, such as vibrations of a drop in partial contact with a 'spherical bowl', the Green's function method has been previously used (Strani & Sabetta 1984). In general, problems with more complex geometries are handled by more computationally intensive approaches (Basaran & DePaoli 1994).

Studies of stability to finite-amplitude disturbances must account for nonlinear effects and, for free boundary problems, the further complication of changes in connectivity. Since any free surface can be plucked to a shape that is nearly pinched off, there are always finite-amplitude disturbances that do not return to the base state. Restrictions on the size and type of disturbances for finite-amplitude stability results are then to be expected. Our characterization of such disturbances depends on the Steiner symmetrization procedure. Whenever the symmetrization is possible,

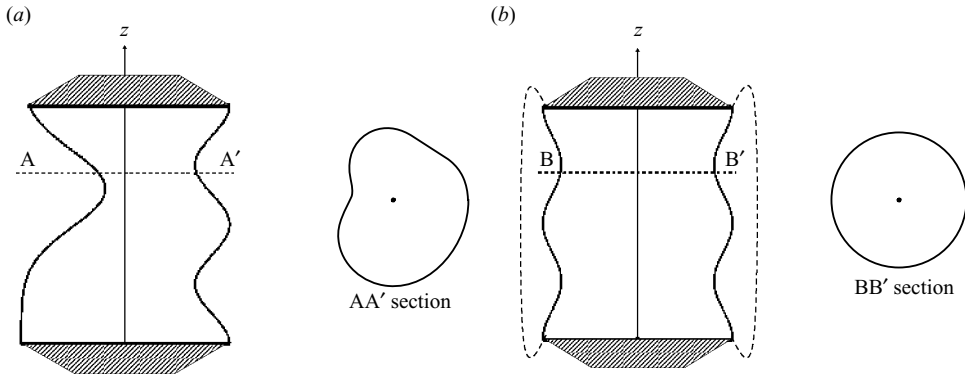


FIGURE 2. Symmetrization of general shape proceeds from (a) non-circular slice AA' to (b) circular slice BB' with reassembly to axisymmetric shape.

it delivers static stability to a class of finite-size disturbances. When symmetrization is not possible, no conclusion can be made.

We first illustrate symmetrization and then its relationship to stability. Consider a liquid bridge spanning endplates where it is pinned along circular contact lines (figure 2). Symmetrization starts with the non-symmetric shape (figure 2a) and ends with the axisymmetric shape (figure 2b). First, take a 'constant z ' cut to obtain the plane figure of section AA' . This AA' figure encloses a planar area. The perimeter of this figure is then minimized, for fixed planar area, to obtain a circle, section BB' . This circle is then reassembled with the circles from other sections, aligning centres, to yield the axisymmetric shape (figure 2b). Symmetrization establishes a mapping from non-axisymmetric to axisymmetric shapes. Gillette & Dyson (1972) proved that this mapping preserves volume while decreasing surface area. Our observation is that their proof allows shape differences to be of finite amplitude. They applied their result to small non-axisymmetric disturbances to conclude that for axisymmetric bridge base states, single valued in radial coordinate, it is sufficient to consider axisymmetric disturbances when testing for stability. That is, if an equilibrium configuration is statically unstable to a non-axisymmetric disturbance, then it is unstable to an axisymmetric disturbance.

Note that the procedure fails if the disturbance section AA' is not simply connected. Such sections certainly occur for base states that are multiple valued in radius, as for the dotted shape in figure 2(b) with slice taken above the top plate. Shapes with tangents to the endplates are the limiting shapes, known as the 'rotund limit' (Russo & Steen 1986). Separate analysis assuming small amplitudes have shown that, beyond the rotund limit, non-axisymmetric disturbances are in fact destabilizing (Slobozhanin, Alexander & Resnick 1997). Hence, failure of the procedure corresponds to a sharp bound. Finally, note that the procedure succeeds even with a solid internal boundary, such as a rod spanning the endplates, as long as the base state and disturbances maintain a fully wetted internal boundary. This occurs, of course, since only increases/decreases in the liquid/gas surface area alter the energy. To use the result of Gillette and Dyson (Gillette & Dyson 1972) for cylindrical interfaces, we lift the cylinder to the torus. Results on finite-amplitude stability of the cylinder are new, as far as we are aware.

The problem we consider is defined by the radius of the cylinder and its axial extent, the polar extent of the cylindrical-cup constraint, and the fill ratio of the

liquid. A comprehensive treatment would study how results depend on fill ratio. To keep the focus on ideas and main results and the paper of modest length, we have suppressed the role of fill ratio. For the dynamics, we restrict to full-cylinder volumes (fill ratio of unity) while for the torus results we indicate how the volume enters when it does. For the symmetrization results, volumes are assumed such that shape meets the support with common tangent, although generalization to other volumes clearly would be straightforward.

In the sections that follow, we first formulate the governing equations, reducing them to linear-operator form, from which a solution is constructed using a Rayleigh–Ritz procedure on a constrained function space. Growth rates and eigenmode structures are then reported. We then lift the cylinder to the torus and focus on wire constraints. Unlike the perfect cylinder, the location of the wire constraint affects the stability. We use symmetrization to establish a finite-amplitude stability result for lens-like cylindrical interfaces and end with concluding remarks.

2. Formulation of dynamical problem

A cylindrical interface of radius R and axial extent L is constrained by a cylindrical-cup solid support, of polar extent $0 \leq \theta \leq \theta_s$, in cylindrical coordinates (r, θ, z) , as shown in figure 1. End-plane boundary conditions are chosen to be (i) the ‘natural’ wetting condition (contact angle of $\pi/2$) equivalent to an infinitely periodic interface or (ii) pinned contact line. The interface of this inviscid fluid is subjected to small time-dependent disturbances of the form $f(\theta, z, t)$. The domain of the liquid bridge is given by

$$D \equiv \{(r, \theta, z) \mid 0 < r \leq R, 0 \leq \theta \leq 2\pi, 0 \leq z \leq L\}. \quad (2.1)$$

Recall that no domain perturbation is necessary for linear problems. The domain (2.1) is bounded by a free-surface (2.2a), the cylindrical-cup (2.2b) and two solid parallel end planes (2.2c):

$$\partial D^f \equiv \{(r, \theta, z) \mid r = R, \theta_s \leq \theta \leq 2\pi, 0 \leq z \leq L\}, \quad (2.2a)$$

$$\partial D_1^s \equiv \{(r, \theta, z) \mid r = R, 0 \leq \theta \leq \theta_s, 0 \leq z \leq L\}, \quad (2.2b)$$

$$\partial D_2^s \equiv \{(r, \theta, z) \mid r = R, 0 \leq \theta \leq 2\pi, z = 0, L\}, \quad (2.2c)$$

$$\partial D^{int} \equiv \partial D^f \cup \partial D_1^s. \quad (2.2d)$$

It is also instructive to define the interface as the union of the free-surface and cylindrical-cup support (2.2d). The fluid of immersion has no inertia and applies a constant pressure on the interface. The effect of gravity is assumed to be negligible.

The Young–Laplace equation,

$$p/\gamma = 2H \equiv \kappa_1 + \kappa_2, \quad (2.3)$$

relates the principal curvatures, κ_1 and κ_2 , of an interface held by surface tension γ (constant, uniform) to the pressure there. A constant pressure is the criteria for static equilibrium, such as $p_0 = \gamma/R$ for a cylinder. Deviations from equilibrium interface configurations generate pressure gradients and thereby flows.

The linearized interface disturbance is constrained by the integral form of the incompressibility condition, which requires the disturbance to be volume conserving

$$\int_0^L \int_0^{2\pi} f(\theta, z) \, d\theta \, dz = 0. \quad (2.4)$$

We consider two end-plane boundary conditions (2.2c). The first is the natural boundary condition for which the contact line is free to move (with contact angle $\pi/2$)

$$\left. \frac{\partial f}{\partial z} \right|_{z=0,L} = 0, \quad (2.5)$$

while the second is a pinned contact line

$$f|_{z=0,L} = 0. \quad (2.6)$$

The flow is assumed to be irrotational and incompressible. The velocity field is described by a velocity potential, $\mathbf{v} = -\nabla\phi$, which satisfies Laplace's equation on the domain (2.1),

$$\nabla^2\phi(r, \theta, z, t) = \frac{1}{r} \frac{\partial}{\partial r} \left(r \frac{\partial\phi}{\partial r} \right) + \frac{1}{r^2} \frac{\partial^2\phi}{\partial\theta^2} + \frac{\partial^2\phi}{\partial z^2} = 0 \quad [D]. \quad (2.7)$$

The kinematic condition

$$v_r = -\frac{\partial\phi}{\partial r} = -\frac{\partial f}{\partial t} \quad [\partial D^f] \quad (2.8)$$

relates the radial component of the velocity to the free-surface deflection. Similarly, the no-penetration condition on the surfaces of support requires

$$v_r = -\frac{\partial\phi}{\partial r} = 0 \quad [\partial D_1^s]; \quad v_z = -\frac{\partial\phi}{\partial z} = 0 \quad [\partial D_2^s]. \quad (2.9)$$

Normal modes are assumed,

$$\phi(r, \theta, z, t) = \phi(r, \theta, z) e^{\beta t}; \quad f(\theta, z, t) = f(\theta, z) e^{\beta t}. \quad (2.10)$$

Substitution of (2.10) into (2.7)–(2.9) yields a boundary value problem for ϕ

$$\nabla^2\phi(r, \theta, z) = \frac{1}{r} \frac{\partial}{\partial r} \left(r \frac{\partial\phi}{\partial r} \right) + \frac{1}{r^2} \frac{\partial^2\phi}{\partial\theta^2} + \frac{\partial^2\phi}{\partial z^2} = 0 \quad [D], \quad (2.11a)$$

$$v_r = -\frac{\partial\phi}{\partial r} = -\beta f(\theta, z) \quad [\partial D^f], \quad (2.11b)$$

$$v_r = -\frac{\partial\phi}{\partial r} = 0 \quad [\partial D_1^s], \quad (2.11c)$$

$$v_z = -\frac{\partial\phi}{\partial z} = 0 \quad [\partial D_2^s]. \quad (2.11d)$$

To solve (2.11), consider boundary conditions (2.11b) and (2.11c) as a single boundary condition on the interface (2.2d) and restrict the 'interface' disturbances to have no amplitude on the surface of support (2.2b). Such constrained interface disturbances satisfy the no-penetration condition (2.11c) by construction and the solution to (2.11) is

$$\phi(r, \theta, z) = -\sum_{m=1}^{\infty} \sum_{l=0}^{\infty} \beta \frac{2}{\pi^2 m} \frac{I_l\left(\frac{m\pi}{L} r\right)}{I_l\left(\frac{m\pi}{L} R\right)} \cos\left(\frac{m\pi}{L} z\right) \xi_l [B_{lm} \cos(l\theta) + C_{lm} \sin(l\theta)], \quad (2.12)$$

where

$$\xi_l = \begin{cases} 1/2 & l = 0, \\ 1 & l \neq 0, \end{cases} \quad (2.13a)$$

$$B_{lm} \equiv \int_0^L \int_0^{2\pi} f(\theta, z) \cos\left(\frac{m\pi}{L}z\right) \cos(l\theta) d\theta dz, \quad (2.13b)$$

$$C_{lm} \equiv \int_0^L \int_0^{2\pi} f(\theta, z) \cos\left(\frac{m\pi}{L}z\right) \sin(l\theta) d\theta dz \quad (2.13c)$$

and I_l is the modified Bessel function of the first kind.

The pressure field is determined from the linearized Bernoulli equation

$$p = p_0 + \rho \frac{\partial \phi}{\partial t} \quad [D], \quad (2.14)$$

where ρ is the fluid density and p_0 is the static pressure required to maintain the fluid's static interface shape. Equating the capillary pressure from (2.3) to the inertial pressure from (2.14) at the interface (2.2d) gives

$$\gamma \left[-\frac{f}{R^2} - \frac{f_{\theta\theta}}{R^2} - f_{zz} \right] = \rho\beta\phi|_{r=R}. \quad (2.15)$$

2.1. Reduction to operator equation

The integrodifferential equation (2.15) is reduced to a problem on the polar component of the interface disturbance $f(\theta, z)$ for natural (defined in (2.5)) and pinned (defined in (2.6)) end conditions.

2.1.1. Natural wetting condition on endplate

To enforce the natural endpoint condition (2.5), a series of solution,

$$f(\theta, z) = \sum_{k=1}^{\infty} A_k(\theta) \cos\left(k\frac{\pi z}{L}\right), \quad (2.16)$$

is used to reduce (2.15) to an integrodifferential eigenvalue problem on $A_k(\theta)$,

$$A_k'' + (1 - \alpha^2)A_k = \sigma^2 \frac{1}{\alpha\pi} \sum_{l=0}^{\infty} \mathcal{J}_l(\alpha) \xi_l [B_l \cos(l\theta) + C_l \sin(l\theta)] \quad (2.17)$$

with

$$\sigma^2 = \rho\beta^2 R^3 / \gamma, \quad (2.18a)$$

$$\alpha = k\pi R / L, \quad (2.18b)$$

$$\mathcal{J}_l(\alpha) \equiv I_l(\alpha) / I_l'(\alpha), \quad (2.18c)$$

$$B_l \equiv \int_0^{2\pi} A_k(\theta) \cos(l\theta) d\theta, \quad C_l \equiv \int_0^{2\pi} A_k(\theta) \sin(l\theta) d\theta. \quad (2.18d)$$

Equation (2.17) is recast as an eigenvalue problem on linear operators

$$K^n [A_k; \alpha] = \sigma^2 M^n [A_k; \alpha], \quad (2.19a)$$

$$K^n [A_k; \alpha] \equiv A_k'' + (1 - \alpha^2)A_k, \quad (2.19b)$$

$$M^n [A_k; \alpha] \equiv \frac{1}{\alpha\pi} \sum_{l=0}^{\infty} \mathcal{J}_l(\alpha) \xi_l [B_l \cos(l\theta) + C_l \sin(l\theta)]. \quad (2.19c)$$

2.1.2. Pinned condition on endplate

An analogous operator equation is derived for the pinned endpoint condition (2.6) using a solution series of the form

$$f(\theta, z) = \sum_{k=1}^{\infty} A_k(\theta) \sin\left(k \frac{2\pi z}{L}\right). \quad (2.20)$$

Substitution of (2.20) into (2.15) produces an integrodifferential equation on $A_k(\theta)$, parameterized by axial wavenumber k , aspect ratio $\hat{\alpha} \equiv \pi R/L$ and formulated as an eigenvalue problem

$$K^P [A_k; \hat{\alpha}, k] = \sigma^2 M^P [A_k; \hat{\alpha}, k], \quad (2.21a)$$

$$K^P [A_k; \hat{\alpha}, k] \equiv A_k'' + (1 - (2k\hat{\alpha})^2) A_k, \quad (2.21b)$$

$$M^P [A_k; \hat{\alpha}, k] \equiv \sum_{m-\text{odd}} \frac{64}{\pi^3 m \hat{\alpha}} \left(\frac{k^2}{4k^2 - m^2} \right) \sum_l \mathcal{J}_l(m\hat{\alpha}) \xi_l [B_l \cos(l\theta) + C_l \sin(l\theta)]. \quad (2.21c)$$

Unlike (2.19a), the pinned operator equation (2.21a) is parameterized by the aspect ratio $\hat{\alpha}$ and discrete axial wavenumber k .

2.1.3. No-penetration auxiliary condition

Solutions of the natural/pinned operator equations are required to satisfy the incompressibility (defined in (2.4)) and no-penetration (defined in (2.11c)) conditions. The solution series for the natural (defined in (2.16)) and pinned (defined in (2.20)) endpoint conditions were chosen to satisfy the incompressibility condition (2.4). However, to ensure the no-penetration condition (2.11c), (2.19a) and (2.21a) are augmented with the following restriction,

$$A_k(\theta) = 0, \quad 0 \leq \theta \leq \theta_s. \quad (2.22)$$

The auxiliary condition (2.22) is satisfied by restricting candidate solutions of (2.19a) and (2.21a) to an appropriately chosen function space.

2.2. Solution of operator equations

The Rayleigh–Ritz procedure for linear operators (e.g. Segel 1987) is used to solve the natural (2.19a) and pinned (2.21a) operator equations, which have the same structural form. The necessary input to such a procedure is a set of orthonormal basis functions, constructed in Appendix, which span a predetermined function space. A solution series

$$A_k(\theta) = \sum_{j=1}^{2N-1} a_j \psi_j(\theta), \quad (2.23)$$

constructed from these orthonormal basis functions ψ_j is used to reduce the eigenvalue operator equation of form $K [A_k] = \sigma^2 M [A_k]$ to a matrix equation,

$$K_{ij} a_j = \sigma^2 M_{ij} a_j, \quad (2.24a)$$

$$K_{ij} \equiv \int_0^{2\pi} K [\psi_i] \psi_j d\theta; \quad M_{ij} \equiv \int_0^{2\pi} M [\psi_i] \psi_j d\theta. \quad (2.24b)$$

The eigenvalues and eigenvectors of (2.24a) are readily computed using standard numerical routines. Eigenvalues and eigenvectors are specified by integer pairs $[l, k]$, the polar and axial wavenumbers, and both depend on the continuous aspect ratio

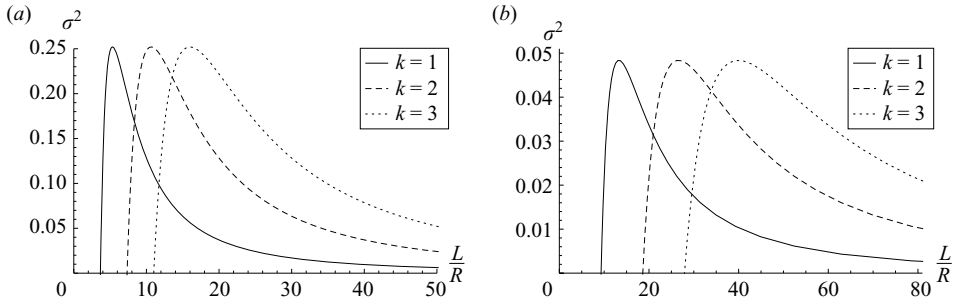


FIGURE 3. Growth rate of most unstable polar mode $[1, k]$ versus aspect ratio L/R : (a) for $\theta_s = 0.01$ with natural conditions and (b) for $\theta_s = 2.0$ for pinned conditions.

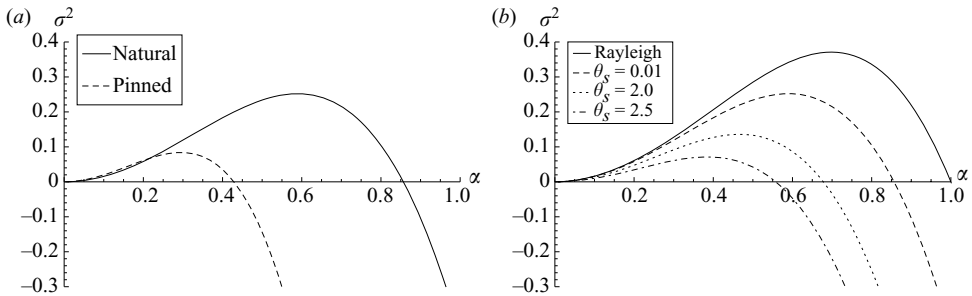


FIGURE 4. Dispersion relation of $l = 1$ modes: (a) for $\theta_s = 0.01$ with natural and pinned conditions and (b) for varying θ_s for natural conditions. Rayleigh dispersion, for reference.

$\pi R/L$. The polar wavenumber is simply the number of intersections plus one of the disturbed circle with undisturbed circle (cf. figure 7). Given an eigenvector $a_j^{(r)}$ of (2.24a), the corresponding eigenfunction is

$$A_k^{(r)}(\theta) = \sum_{j=1}^{2N-1} a_j^{(r)} \psi_j(\theta). \tag{2.25}$$

3. Results for a constrained cylindrical interface

The eigenvalues/eigenmodes of the operator equations (2.19a) and (2.21a) are computed using standard numerical routines for a fixed constraint size θ_s . All eigenvalues presented here show convergence to within 0.1 %, when 13 terms ($N = 7$) have been used in the solution series (2.23). The eigenvalues for the most unstable polar mode ($l = 1$) depend on aspect ratio as shown in figure 3, for various axial wavenumbers k . As seen from the natural operator (2.19a), L/R and k are not independent and the separate curves collapse onto a single curve by scaling. In contrast, because L/R and k appear separately in the pinned operator (2.21a), they appear to be independent but the same scaling also collapses the curves in figure 3(b) so, in fact, they are not independent.

Relative to the natural end constraint, the pinned end constraint always increases static stability α_c by a factor of two and this is shown for the touching wire in figure 4(a). Increasing the polar constraint also always stabilizes, as shown for the natural conditions in figure 4(b). These static stability results are summarized in

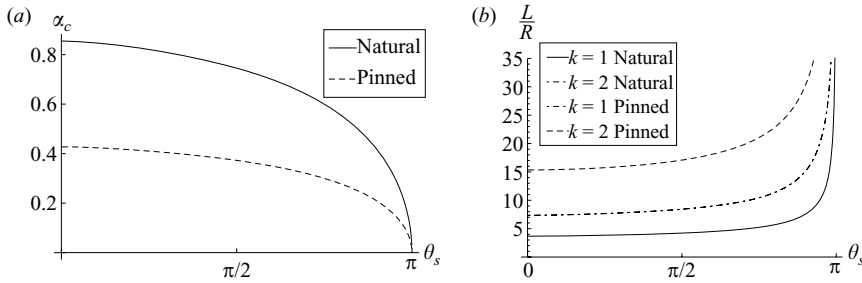


FIGURE 5. Static stability against polar constraint θ_s measured by (a) wavenumber α_c or (b) envelope of stable L/R (below curve).

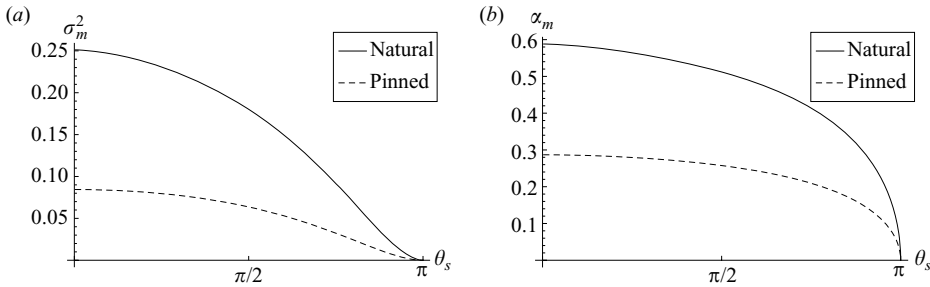


FIGURE 6. (a) Growth rate σ_m^2 and (b) wavenumber α_m against polar constraint for fastest growing mode.

figure 5. The curve for natural end conditions on figure 5(a) recovers (1.2) and could be read off figure 4(b). The pinned curve on figure 5(a) is the natural curve scaled by a factor of two. This relationship between the pinned and natural stability limits is seen again in figure 5(b), which plots the static limit as it depends on the length and polar constraints, the so-called stability envelope. There, the $k=1$ pinned and $k=2$ natural curves collapse to a single curve and the $k=1$ pinned and $k=1$ natural curves differ by a factor of 2. Indeed, the four curves of figure 5(b) all collapse onto a single curve. We have plotted them separately to compare directly to the natural end-constraint results of Brown & Scriven (1980), with which they are in agreement. The convergence of eigenvalue/eigenmodes and the recovery of a range of static stability results are tests that validate the computations.

Each dispersion relation seen in figure 4 exhibits a fastest growing mode with corresponding aspect ratio which, following Rayleigh, can be interpreted as an estimate for the bead size which results from the breakup instability. Figure 4(b) shows that the maximum growth rates of the unstable modes are smaller than that for the corresponding unconstrained Rayleigh jet ($\sigma_{Ray}^2 = 0.343$). The Rayleigh dispersion relation is plotted for reference. Figure 6 summarizes the maximum growth rates (figure 6a) and corresponding aspect ratios (figure 6b) as they depend on extent of support. Figure 7(a) illustrates the mode shape of a pinned-end disturbance, unstable when unconstrained, but stabilized by a cup that is 63.7% of the critical cup (π). For the same constraint, figure 7(b) shows the [3, 2] vibrational mode (stable). Increasing the polar constraint stabilizes, as mentioned. However, slower growing unstable modes remain and such a mode shape is illustrated in figure 7(c) for natural-end conditions in the presence of a wire constraint. Figure 7(d) shows the [2, 3] vibrational mode (stable) for a wire constraint.

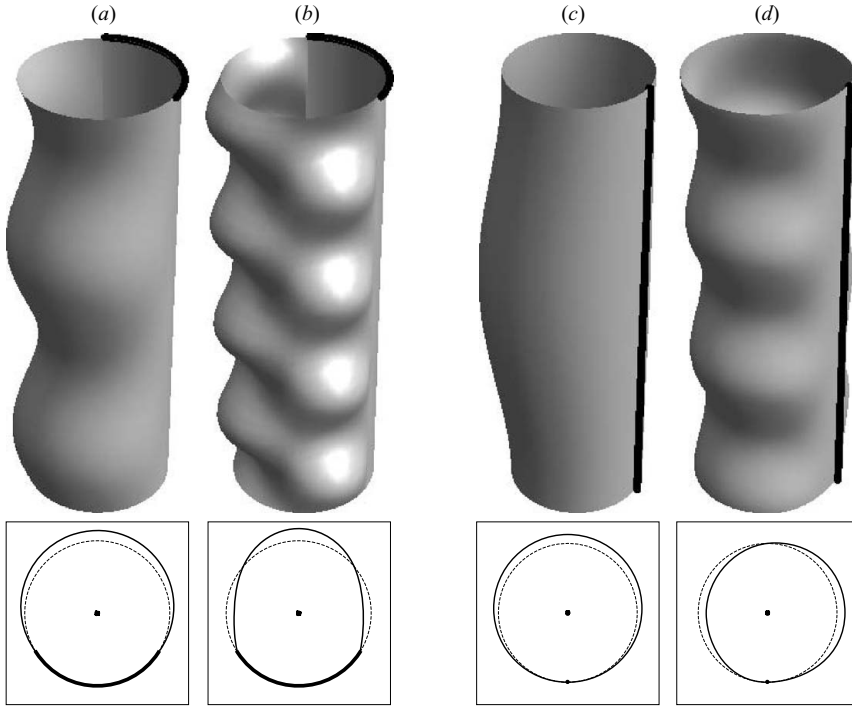


FIGURE 7. Modes $[l, k]$ in three-dimensional and polar views for $L/R = 2\pi$ with (a, b) $\theta_s = 2.0$ and pinned conditions for (a) $[1,1]$ and (b) $[3,2]$ and (c, d) $\theta_s = 0.01$ and natural conditions for (c) $[1,1]$ and (d) $[2,3]$.

Explicit knowledge of the inertia operator $M[y]$ is needed to determine the spectrum of the eigenvalue problem (2.24a), but is not necessary to show static stability, provided one can show $(M[y; \alpha], y) > 0$ for $y \neq 0$. Indeed, if $M[y; \alpha]$ is positive definite, the curvature operator $K[y; \alpha]$ determines the sign of the eigenvalues and may be used to determine the static stability limit α_c . Positive definiteness of M is straightforward to show and we sketch the argument. Applying Green's first identity to the velocity potential $\phi(\mathbf{x})$ on the domain D , results in an integral over the domain and its boundary,

$$\int_{\partial D} \phi (\nabla \phi \cdot \mathbf{n}) \, dS = \int_D [\phi \nabla^2 \phi + \nabla \phi \cdot \nabla \phi] \, dV. \tag{3.1}$$

The domain integral is evaluated using $\nabla^2 \phi = 0$. The boundary integral is evaluated using $\phi|_{\partial D} = M[y]$, which follows from the linearized Bernoulli equation, and using $\nabla \phi \cdot \mathbf{n} = y$, which follows from the kinematic condition.

For the axial and polar constraints considered so far, narrowing the class of disturbances enhances stability. Next we enlarge the class of equilibrium states and show that, relative to the cylindrical cap interface, constraint can be stabilizing or destabilizing.

4. Lifting the cylinder to the torus

The torus with surface of revolution constraint is of interest (cf. figure 8). The torus is described using a standard parametric representation (e.g. Kreyszig 1991),

$$x = (R + a \cos \theta) \cos \varphi, \quad y = (R + a \cos \theta) \sin \varphi, \quad z = a \sin \theta. \tag{4.1}$$

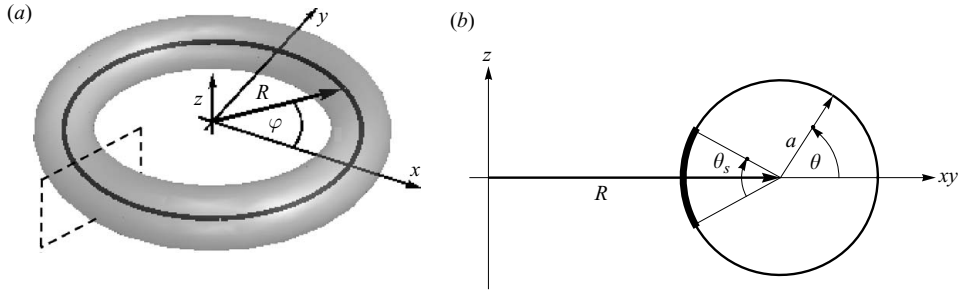


FIGURE 8. Torus sketch in (a) three-dimensional view and in (b) polar view with cup support (thick line).

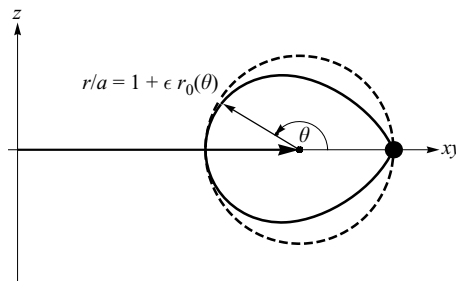


FIGURE 9. Torus equilibrium shape $r_0(\theta)$ with unit circle for reference (dotted).

The torus is a near cylinder for $\epsilon \equiv a/R \ll 1$ and, in the limit $\epsilon \rightarrow 0$, a cylinder with axial periodicity. An in-plane bending of the constraint introduces a secondary curvature, controlled by ϵ . A straightforward calculation of the mean curvature H of the torus (defined in (4.1)) shows that it varies with θ according to $a(2H) = 1 + \epsilon(\cos\theta/(1 + \epsilon \cos\theta))$. A non-constant mean curvature does not satisfy the Young–Laplace law and, hence, the torus surface is not in capillary equilibrium.

For the near-cylindrical torus, however, a near-toroidal shape can be found that is an equilibrium shape provided that the shape is constrained. It turns out that such a constraint must be symmetric about the $z=0$ mid-plane. For this reason, we focus on constraints symmetric about the mid-plane and, analogous to those considered for the cylinder, subtending an angle θ_s . This constraint is either ‘inside’ (as in figures 8 and 10b) or ‘outside’ (as in figure 9b) relative to the origin. In the limiting case $\theta_s = 0$, the constraint is a wire. In the further limit of $\epsilon = 0$, the perfect cylinder is recovered and the distinction between inside and outside is lost.

We refer to the family of near-toroidal equilibrium shapes as the ‘torus lift of the cylinder’; the family is parameterized by ϵ . The torus lift is of interest for two different kinds of results, both regarding static stability. Firstly, we calculate stability of the torus lift to small disturbances for the case of inner and outer wire constraints. This suffices to demonstrate the destabilizing and stabilizing nature of the inner and outer constraints, respectively. Secondly, we restrict to cylindrical lens-like shapes ($\theta_s > \pi$) and use Steiner symmetrization on the torus lift to demonstrate stability to finite-amplitude disturbances. The limiting case $\theta_s = \pi$ is seen to be a ‘hard’ stability boundary.

4.1. Near-toroidal equilibrium shapes

Lengths can be scaled by a so small deformations take the form (cf. figure 8),

$$r/a = 1 + \epsilon r_0(\theta). \quad (4.2)$$

Here, in view of the mean curvature of the perfect torus, shapes depending only on θ are anticipated. The strategy is to seek near-toroidal shapes that just cancel the curvature of the torus. At order ϵ , the near-cylindrical and near-toroidal curvatures are found to be $\cos \theta/a$ and $-(r_0 + r_0'')/a$, respectively. Hence, to this order, equilibrium is maintained provided

$$r_0'' + r_0 = \cos \theta. \quad (4.3)$$

Solution to (4.3) is given by

$$r_0(\theta) = 1/2(\theta - \pi) \sin \theta, \quad (4.4)$$

where boundary conditions symmetric about the mid-plane corresponding to the outer wire constraint have been enforced. This particular shape is shown in figure 9. The shape has a corner at the wire ($\theta = 0, 2\pi$). The corner may be shifted from the outer to the inner position by redefining the polar surface coordinate $\theta \rightarrow \theta - \pi$ and using an alternative solution to (4.3), $r_0 = 1/2(\theta - \pi) \sin(\theta - \pi)$.

Note that a slightly larger class of solutions would be obtained by adding a constant to the right-hand side of (4.3). This corresponds to allowing near-toroidal equilibrium shapes with 'constant' mean curvatures of a different 'constant' than the cylinder. Physically, this amounts to an adjustment of the volume of liquid. In summary, if one demands that the volume of the equilibrium shape be the same as that of the corresponding near-cylindrical shape, it can be arranged, although there is no fundamental reason to do so. Finally, volumes can be easily calculated by Pappus' theorem knowing the centroid of the plane figure and its planar area.

4.2. Stability of near-toroidal equilibrium shapes

The equilibrium shape is perturbed by an amount δ of the form $r_1(\theta, \varphi)$

$$r/a = 1 + \epsilon r_0 + \delta r_1(\theta) e^{iq\varphi}, \quad (4.5)$$

where q is the toroidal azimuthal wavenumber. The disturbance must remain smaller than the deviation from the cylinder, $\delta \ll \epsilon$. Note that the disturbance preserves volume of the equilibrium state.

Static stability of the base state is determined by the order δ deviation of the mean curvature. This deviation, as it depends on ϵ , is formulated as an operator

$$K[r_1; \alpha, \epsilon] \equiv (2H)_\delta = [(1 + \epsilon \cos \theta)^2 + \epsilon^2 \cos \theta - \alpha^2] r_1 \mp \epsilon(1 + \epsilon \cos \theta) \sin \theta r_1' + (1 + \epsilon \cos \theta)^2 r_1'' - \epsilon^2(1 + \epsilon \cos \theta)^2 F[\theta], \quad (4.6)$$

where $\alpha = qa/R$ is the scaled wavenumber and

$$F[\theta] \equiv \frac{1}{16}[-3 - (\theta - \pi)^2 + ((\theta - \pi)^2 - 13) \cos 2\theta + 14(\theta - \pi) \sin 2\theta]. \quad (4.7)$$

Allowable solutions of (4.6) are subject to the no penetration condition along the wire constraint

$$r_1(\theta = 0, 2\pi) = 0. \quad (4.8)$$

The \mp signs in (4.6) denote a torus with an outer or inner wire constraint, respectively.

Static stability is determined by the sign of the curvature operator ($K[y; \alpha], y$), where the surface disturbance y belongs to an appropriate function space. Allowable

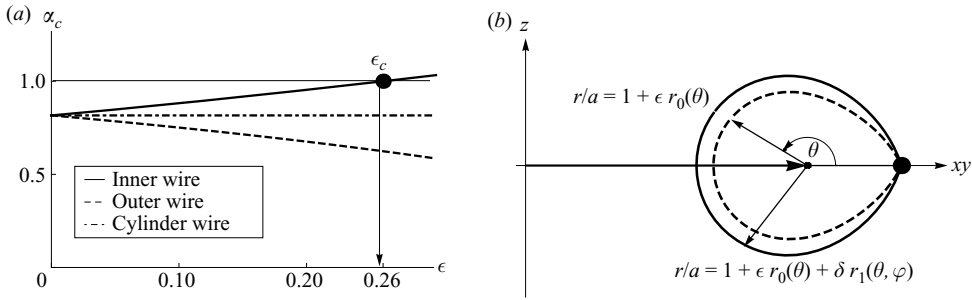


FIGURE 10. Stability of toroidal equilibrium shapes showing (a) static limit α_c against deviation from cylinder ϵ and (b) typical destabilizing mode shape, with equilibrium shape for reference (dotted).

surface disturbances to the torus must satisfy (4.8), which are structurally identical to the free-surface disturbances of the cylinder with a wire constraint. Therefore, the solution series (2.23) derived earlier can be used as the input to the Rayleigh–Ritz procedure on the curvature operator (4.6) for the torus. Also note that the curvature operator (4.6) reduces to the curvature operator for the cylinder (see (2.19b)) in the limit $\epsilon \rightarrow 0$.

Given α and ϵ , the spectrum of $K[r_1; \alpha, \epsilon] = \sigma^2 r_1$ is readily computed using the Rayleigh–Ritz procedure. For secondary curvature ϵ , the critical wavenumber α_c is computed by iterating over α and locating where the unstable eigenvalue changes sign.

Figure 10(a) plots the critical wavenumber versus secondary curvature for a torus with a wire constraint placed on the inner and outer extrema. Figure 10(b) displays the polar projection of the instability mode shape. Figure 10(a) shows that the location of the wire constraint can have either a stabilizing (outer pin) or destabilizing (inner pin) effect, when compared to the wire-constrained cylinder. For the inner pin, as the secondary curvature increases, a cancellation occurs at $\epsilon_c = 0.26$, where the destabilizing effect of the secondary curvature exactly cancels the stabilization of the wire inherited from the cylinder. The toroidal equilibrium shape of this size with inner wire constraint will have precisely the Plateau–Rayleigh limit. The validity of the expansion to ϵ_c and beyond is plausible in view of the linear dependence seen in figure 10(a) but has not been investigated further.

4.3. Symmetrization and large-amplitude stability of the lens meniscus

As described in §1, symmetrization uses a cylindrical coordinate system and takes plane slices orthogonal to the generator axis, which we shall call the *symmetrization axis* (figure 1). Symmetrization can proceed if the slices yield a simply-connected planar figure. This occurs precisely when starting with a single-valued volume-enclosing shape. This motivates the notion of finite-amplitude ‘admissible’ interfaces – interfaces that are single valued in the radial direction relative to the symmetrization-axis. To obtain stability results, both base state and disturbances must be admissible.

The equilibrium interfaces of the torus lift family are admissible for $\theta_s > \pi$ for a range of volumes. These are lens-like meniscus shapes. Recall the result of Gillette & Dyson (1972): symmetrization maps non-axisymmetric shapes onto axisymmetric shapes of the same volume but with lesser surface area (GD reduction theorem). This applies directly to the torus lift. Hence, to obtain stability to general volume-preserving admissible disturbances, it is *sufficient to consider axisymmetric disturbances*, relative

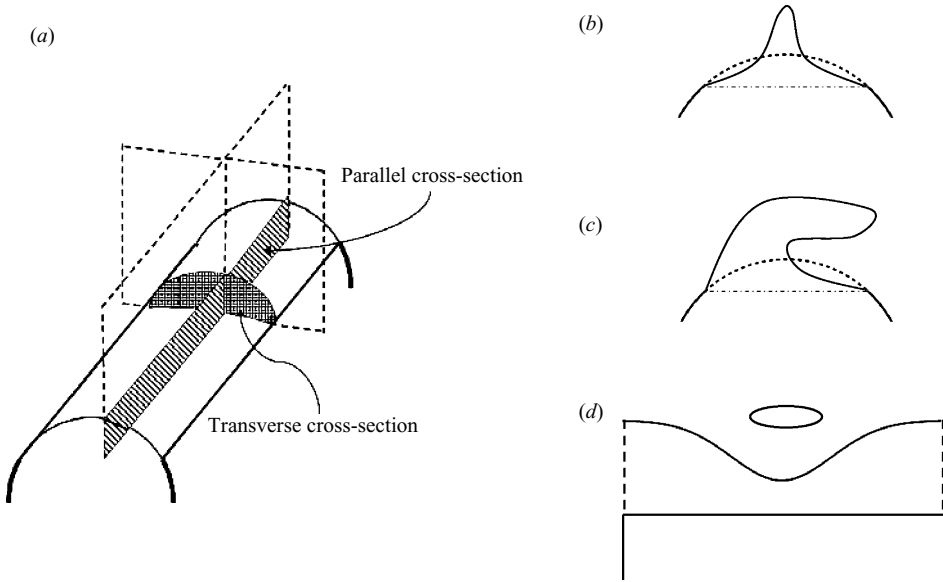


FIGURE 11. Symmetrization of lens meniscus using (a) parallel and transverse cross-sectional slices in three-dimensional view; sketches of large-amplitude disturbances that are (b) admissible (in transverse section) or (c, d) inadmissible; (c) in transverse section, (d) in parallel section.

to the symmetrization axis. These are the most dangerous. This reduces the full three-dimensional problem to a two-dimensional planar one. Of course, the reduction fails for multiple-valued base states; these do occur for $\theta_s < \pi$ and a filling ratio of unity. The reader should be reminded that volume, an independent parameter, is taken to be the filling volume in this paper, for efficiency of presentation. Note that, for a fixed $\theta_s < \pi$, there will be a range of volumes (low) that have single valued and a range (modest to high) that have double-valued equilibrium shapes. The filling volume is that volume whose equilibrium shape meets the constraint at the contact line tangentially.

Symmetrization of the torus lift can deliver *general* large-amplitude stability results in the limit of the cylindrical-lens meniscus (figure 11). That is, in the cylindrical limit $\epsilon = 0$, the toroidal equilibrium shapes reduce to cylindrical cap shapes and, for $\theta_s > \pi$, these are cylindrical lenses. The GD reduction theorem applies to each $\epsilon > 0$ and thus holds in the limit $\epsilon = 0$. The toroidal equilibrium shape is relatively stable to axisymmetric disturbances (finite amplitude, admissible, volume preserving) and, hence, the cylindrical lens is relatively stable to disturbances varying in parallel cross-sections (figure 11a). It is left to show that the lens is also relatively stable to disturbances in the transverse plane. This follows by choosing a new symmetrization axis – the axis of the cylindrical meniscus – for which slices are transverse cross-sections (figure 11a), and applying the GD theorem again. One then concludes that disturbances with variations along parallel cross-sections are most dangerous. Together, the results from orthogonal symmetrization procedures, delivers the result; the cylindrical lens is stable to general large-amplitude volume-preserving admissible disturbances. It remains to state this result formally.

Disturbance class. ‘Admissible’ interface shapes are those with parallel and transverse cross-sections that are simply connected. (An equivalent definition is those shapes that

are single valued in the radial coordinate, relative to both symmetrization axes; that is, both parallel and transverse slices give single-valued shapes.)

Figure 11(b) illustrates a large-amplitude disturbance (transverse section) that is admissible while figure 11(c,d) give orthogonal views of an inadmissible disturbance.

THEOREM 1. *The cylindrical interface of cylindrical volume, constrained by solid support $\theta_s > \pi$ with pinned contact lines, is statically stable to arbitrarily large volume-preserving disturbances as long as the disturbances are admissible and preserve wetted area of contact with the solid support.*

This theorem is proved by observing that (i) the GD reduction theorem applies to large-amplitude disturbances, (ii) the GD reduction applies to the lens-like toroidal equilibrium states (inside constraint), (iii) the toroidal azimuthal coordinate becomes the cylindrical axial coordinate in the cylindrical limit of the torus and that (iv) the GD reduction also applies with the toroidal axial coordinate as symmetrization axis. In summary, the cylindrical lens base state admits symmetrization in two orthogonal directions, by which it is found to be globally stable to admissible disturbances. Our theorem says that $\theta_s > \pi$ is *sufficient* for stability of the cylindrical interface while the linear stability results in the literature show that $\theta_s \geq \pi$ is also *necessary* for stability since, for $\theta_s < \pi$, small disturbances that destabilize have been exhibited.

5. Concluding remarks

Constraint tends to stabilize, whether via end plane (axial) or lateral cup (polar). To the extent that a constraint narrows the class of disturbances to which a base state is subject, this stands as a principle. In going from the natural to the pinned end-plane conditions, the instability window is narrowed by a factor of two no matter the extent of the cup constraint. In going from the unconstrained cylinder (Plateau–Rayleigh) to the cylinder touching a wire, the instability window is narrowed by 13%. Increasing θ_s narrows the instability window further until it disappears at $\theta_s = \pi$ and beyond which it remains closed. All this is known from prior work. In contrast, bending the cup constraint into a torus configuration can either stabilize or destabilize depending on whether the cup is placed on the inside or outside of the bend. Bending creates two new families of equilibrium states. For each member of these families, increasing the constraint will enhance stability, while relative to the constrained cylinder the new family can be more or less stable. We have shown how the destabilization of bending curvature can cancel the stabilization of the wire to yield the same critical value as occurs for the Plateau–Rayleigh instability. All these are small-amplitude static results.

The torus lift of the cylinder helps us prove a large-amplitude stability result for cylindrical lens interfaces ($\pi < \theta_s < 2\pi$). Large disturbances, just so they are single valued, are statically stable. This may provide important insight for application. For example, one way to discourage multiple-valued disturbances is to limit the liquid volume. Furthermore, as a tool for obtaining finite-amplitude results, the symmetrization technique may well be useful to a broader class of interfacial stability problems.

As regards dynamics, we solve the disturbance equations posed by Davis (1980) in the special case of an inviscid liquid when the liquid is pinned along the edges of the circular cup and of a volume that just fills the circular section. An integrodifferential equation has been derived for both natural and pinned axial constraints. The governing equation is formulated as an eigenvalue problem on linear

operators, from which a solution is constructed using a Rayleigh–Ritz procedure. The eigenvalues/eigenmodes are dependent upon the polar constraint and have been computed from a truncated set of linear algebraic equations using standard numerical routines.

All the lens-like interfaces are always stable; only oscillatory motions occur. These vibrational modes may be of practical relevance for coating ‘beads’ and casting processes, but a comparison with experiment is beyond the scope of this paper. For the drop-like interfaces, only the eigenmode with smallest polar wavenumber $l = 1$ exhibits instability and that for a range of axial wavenumbers. The polar constraint stabilizes axial wavenumbers that are unstable for the Plateau–Rayleigh cylinder, as mentioned. The constraint also slows the growth rate of the unstable modes but the slowing of growth rates does not scale in the same manner as the static limit stabilization. For example, the disturbance with fastest growth rate for the natural end-point conditions grows nearly three times as fast as that of the corresponding pinned end-point mode. The cylinder against a wire illustrates the influence of constraint. Compared to Rayleigh breakup, the fastest growing disturbance is 18 % longer suggesting about a 6 % increase in final droplet size. What might be easier to distinguish in experiment is that the characteristic time to breakup is nearly 40 % longer for the wire constraint as compared to the unconstrained Rayleigh breakup. We are unaware of any reports of experiments that would allow comparison, however.

This work was supported by NSF grant CMMI 0726813 and NASA grant NNX09AI83G.

Appendix. Constrained function space construction

To construct the constrained function space, begin by considering candidate functions of the form

$$A_k(\theta) = \begin{cases} 0 & 0 \leq \theta \leq \theta_s, \\ y(\theta) & \theta_s \leq \theta \leq 2\pi. \end{cases} \quad (\text{A } 1)$$

By definition, functions of the form (A 1) satisfy (2.22). To ensure the interface perturbation $A_k(\theta)$ is single valued, the following conditions are placed on the free-surface deformation $y(\theta)$,

$$y(\theta_s) = 0; \quad y(2\pi) = 0. \quad (\text{A } 2)$$

Next, assume the free-surface deformation $y(\theta)$ may be expressed as

$$y(\theta) = \sum_{j=0}^N b_j \cos(j\theta) + c_j \sin(j\theta). \quad (\text{A } 3)$$

Substituting (A 3) into (A 2) gives

$$\begin{bmatrix} 1 \cos(\theta_s) \cdots \cos(N\theta_s) \sin(\theta_s) \cdots \sin(N\theta_s) \\ 1 \quad 1 \quad \cdots \quad 1 \quad 0 \quad \cdots \quad 0 \end{bmatrix} \begin{bmatrix} b_0 \\ \vdots \\ c_N \end{bmatrix} = \begin{bmatrix} 0 \\ 0 \end{bmatrix} \quad (\text{A } 4)$$

or a set of algebraic equations on the coefficients of the test function series (A 3). There exists $2N - 1$ coefficient vectors that solve (A 4), or $2N - 1$ linearly independent functions of the form (A 3) that solve (A 2). The Gram–Schmidt orthogonalization procedure and a computer algebra package are used to convert the linearly

independent basis functions into a set of orthonormal functions $\{\psi_j(\theta)\}$, which span the constrained function space.

REFERENCES

- BASARAN, O. & DEPAOLI, D. 1994 Nonlinear oscillations of pendant drops. *Phys. Fluids* **6**, 2923–2943.
- BOSTWICK, J. B. & STEEN, P. H. 2009 Capillary oscillations of a constrained liquid drop. *Phys. Fluids* **21**, 032108.
- BROWN, R. A. & SCRIVEN, L. E. 1980 On the multiple equilibrium shapes and stability of an interface pinned on a slot. *J. Colloid Interface Sci.* **78**, 528–542.
- BYRNE, C. J., THEISEN, E. A., REED, B. L. & STEEN, P. H. 2006 Capillary puddle vibrations linked to casting-defect formation in planar-flow melt spinning. *Metall. Mater. Trans. B* **37B**, 445–456.
- DAVIS, S. H. 1980 Moving contact lines and rivulet instabilities. Part 1. The static rivulet. *J. Fluid Mech.* **98**, 225–242.
- DEEGAN, R. D., BRUNET, P. & EGGERS, J. 2008 Complexities of splashing. *Nonlinearity* **21**, C1–C11.
- GILLETTE, R. D. & DYSON, D. C. 1972 Stability of axisymmetric liquid-fluid interfaces towards general disturbances. *Chem. Engng J.* **3**, 196–199.
- KREYSZIG, E. 1991 *Differential Geometry*. Dover.
- LAMB, H. 1932 *Hydrodynamics*. Cambridge University Press.
- LANGBEIN, D. 1990 The shape and stability of liquid menisci at solid edges. *J. Fluid Mech.* **213**, 251–265.
- LOWRY, B. J. & THIESSEN, D. B. 2007 Fixed contact line helical interfaces in zero gravity. *Phys. Fluids* **19**, 022102.
- LYUBIMOV, D. V., LYUBIMOVA, T. P. & SHKLYAEV, S. V. 2006 Behaviour of a drop on an oscillating solid plate. *Phys. Fluids* **18**, 012101.
- MAJUMBAR, S. R. & MICHAEL, D. H. 1976 The equilibrium and stability of two-dimensional pendent drop. *Proc. R. Soc. Lond. A* **351**, 89–115.
- MAY, H. J. & LOWRY, B. J. 2008 Microgravity/microscale double-helical fluid containment. *Proc. R. Soc. A* **464**, 855–875.
- MICHAEL, D. H. 1981 Meniscus stability. *Annu. Rev. Fluid Mech.* **13**, 189–215.
- MYSHKIS, A. D., BABSII, V. G., SLOBOZHANIN, N. D. & TYUPTSOV, A. D. 1987 *Low-Gravity Fluid Mechanics*. Springer.
- PLATEAU, J. A. F. 1863 Experimental and theoretical researches on the figures on equilibrium of a liquid mass withdrawn from the action of gravity. *A. Rep. Board Reg. Smithsonian. Inst.* pp. 207–285.
- RAYLEIGH, LORD 1879 On the capillary phenomenon of jets. *Proc. R. Soc. Lond.* **29**, 71–97.
- RENARDY, Y., POPINET, S., DUCHEMIN, L., RENARDY, M., ZALESKI, S., JOSSEAND, C., DRUMRIGHT-CLARKE, M. A., RICHARD, D., CLANET, C. & QUÈRÈ, D. 2003 Pyramidal and toroidal water drops after impact on a solid surface. *J. Fluid Mech.* **484**, 69–83.
- ROY, R. V. & SCHWARTZ, L. W. 1999 On the stability of liquid ridges. *J. Fluid Mech.* **391**, 293–318.
- RUSSO, M. J. & STEEN, P. H. 1986 Instability of rotund capillary bridges to general disturbances: experiment and theory. *J. Colloid Interface Sci.* **113**, 154–163.
- SEGEL, L. A. 1987 *Mathematics Applied to Continuum Mechanics*. Dover.
- SLOBOZHANIN, L., ALEXANDER, J. I. D. & RESNICK, A. 1997 Bifurcation of the equilibrium states of a weightless liquid bridge. *Phys. Fluids* **9**, 1893–1905.
- STEEN, P. H. & KARCHER, C. 1997 Fluid mechanics of spin casting. *Annu. Rev. Fluid Mech.* **29**, 373–397.
- STEINER, J. 1882 *Gesammelte Werke*. Reimer.
- STRANI, M. & SABETTA, F. 1984 Free vibrations of a drop in partial contact with a solid support. *J. Fluid Mech.* **141**, 233.
- THIESSEN, D. B., BERNATE, J. & MARSTON, P. L. 2005 Capillary-driven flow in supported capillary pipes. *AIChE Annual Meeting*. Oct. 30–Nov. 4, 2005, Cincinnati, OH (paper 124f).
- WEILAND, R. H. & DAVIS, S. H. 1981 Moving contact lines and rivulet instabilities. Part 2. Long waves on flat rivulets. *J. Fluid Mech.* **107**, 261–280.